THE JOURNAL OF PHYSICAL CHEMISTRY C
A JOURNAL OF THE AMERICAN CHEMICAL SOCIETY



pubs.acs.org/JPCC
Article

# Resistance of Boron Nitride Nanotubes to Radiation-Induced Oxidation

Hsin-Yun Chao, Adelaide M. Nolan, Alex T. Hall, Dmitri Golberg, Cheol Park, Wei-Chang David Yang, Yifei Mo, Renu Sharma, and John Cumings*

Cite This: J. Phys. Chem. C 2024, 128, 18328−18337

Read Online

ACCESS | Metrics & More | Article Recommendations | Supporting Information

**ABSTRACT:** We present unprecedented results on the damage thresholds and pathways for boron nitride nanotubes (BNNT) under the influence of energetic electrons in an oxidative gas environment, using an environmental aberration-corrected electron microscope over a range of oxygen pressures. We observe a damage cascade process that resists damage until a higher electron dose, compared with carbon nanotubes, initiating at defect-free BNNT sidewalls and proceeding through the conversion from crystalline nanotubes to amorphous boron nitride (BN), resisting oxidation throughout. We compare with prior results on the oxidation of carbon nanotubes and present a model that attributes the onset of damage in both cases to a physisorbed oxygen layer that reduces the threshold for damage onset. Surprisingly, increased temperatures offer protection against damage, as do electron dose rates that significantly exceed the oxygen dose rates, and our model attributes both effects to a physisorbed oxygen population.

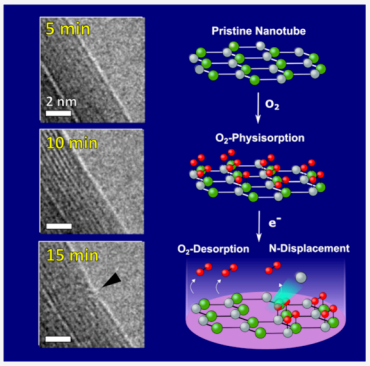


## 1. INTRODUCTION

Radiation-resistant materials are essential to prevent harmful irradiation effects on Earth and in space.[1,2] Boron nitride nanotubes (BNNT), apart from having superior structural properties such as a high elastic modulus[3] and thermal resistance in air,[4] also have potential as a radiation-resistant material.[5,6] Boron-based, low atomic number materials have often been exploited for their capabilities for radiation prevention with resistance to secondary radiation and a high neutron absorption cross section.[7,8] Transmission electron microscopes (TEM) are the preferred instruments to explore nanoscale interactions due to their ever-improving atomic and subatomic resolution capabilities.[9,10] Specifically, nanotubes have been studied extensively inside the TEM looking at their structure,[11] chirality,[12] and electronic properties.[13] Though electron irradiation has largely been viewed as an unintended consequence in the TEM,[14] it effectively mimics ionizing particle-induced degradation encountered in real-world settings. TEM techniques for creating a controlled experiment include temperature regulation (heating and cooling),[15,16] biasing (electric field),[17] and environmental capabilities (liquid and gas).[18] In particular, an environmental TEM (ETEM) that regulates gas flow through a dedicated port can create customized gas environments around the sample, without requiring a specialized holder. Previously, ETEM has been utilized to study carbon nanotubes (CNT), including growth,[19−21] chirality,[22] catalyst deactivation,[23] and beam-induced transformations.[24−26]

Experiments on beam-induced damage have produced a number of useful models to describe and predict the damage rates and mechanisms, under high-vacuum conditions.[27−29] The most prominent types of damage mechanisms observed on thin samples in the TEM consist of both inelastic effects such as Coulombic charging and radiolysis and elastic effects dominated by knock-on damage and atomic displacement.[27,30] Inelastic effects of monolayer hexagonal boron nitride (h-BN) are explored by Cretu et al. and hypothesized to mainly consist of Coulombic charging as excitons in h-BN[31] are lower than the minimum displacement threshold needed for radiolysis.[32,33] In addition, heating experiments done at elevated temperatures between 500 and 1200 °C show an increase in damage with temperature.[32] Kotakoski et al. report elastic knock-on energy thresholds for B and N from molecular dynamics (MD) simulations of an h-BN monolayer, with confirmation from TEM results.[33] For h-BN in high vacuum, B is observed to have a lower damage threshold, and the generated vacancies are N-terminated, which is corroborated by scanning transmission electron microscopy (STEM)[34] and high-resolution TEM (HRTEM) studies.[35,36] Models comparing damage cross sections for both knock-on and radiolysis of h-BN[32,37] are supported by experimental results,[32,35,36,38−40] but the scope of the studies has been limited to h-BN under high vacuum. Moreover, recent TEM degradation studies on

Received: June 7, 2024
Revised: September 19, 2024
Accepted: September 20, 2024
Published: October 22, 2024

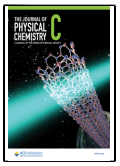

graphene and 2D materials have also been instructive for understanding damage via electron beam.[41−43]

To understand the damage mechanisms of BNNT in an oxidative environment, we found a direct comparison to carbon nanotubes critical because BNNT has not had prior ETEM investigations conducted under $O_2$ gas conditions as CNT does. Koh et al. thoroughly investigated CNT inside the ETEM during oxidation by $O_2$ gas.[24,44,45] Cumulative electron dose initiating the damage is measured for multiwalled CNT (MWCNT)[45] at room temperature as well as at elevated temperatures.[44] By varying $O_2$ dose, the associated electron dose necessary for damage at higher $O_2$ pressure ranges is obtained.[24] A 2 orders of magnitude increase in the electron dose threshold from $10^4$ to $10^6$ $e^-/Å^2$ for initial nanotube damage at high vacuum (lowest $O_2$ gas pressure) compared to highest $O_2$ gas pressure measured is reported. These initial damage events are followed by a cascade process in which an amorphous BN region is observed to grow with time during e-beam illumination. Additionally, an increase in temperature from room temperature to 300 °C results in decreasing the damage cascade from 24 to 0.16 atom/s.[45] This indicates an increase in resistance to electron-induced degradation with temperature increase.

In this paper, we aim to give systematic insight into the knock-on damage phenomenon for BNNT at an electron energy of 80 keV, which is below the established thresholds for knock-on damage for graphite[27] and h-BN.[33] At this electron energy, we expect that BNNT will not readily damage in a vacuum but will damage in the presence of $O_2$ gas. We employ ETEM to explore oxygen-assisted damage by varying $O_2$ pressure in the specimen chamber, accompanied by heating experiments where $k_BT$ is greater than the desorption energy of $O_2$. Furthermore, we use ab initio molecular dynamics (AIMD) simulations to provide electron and nuclear threshold energies for single- and double-layer graphene and h-BN and elucidate underlying mechanisms. The combination of experimental and computational work allows us to evaluate the resistance to electron radiation of BNNT compared to CNT, to uncover the change in electron displacement threshold with an adsorbed $O_2$ monolayer, and to formulate a knock-on damage pathway through $O_2$ physisorption.

## 2. MATERIALS AND METHODS

**2.1. Experiments.** The specimen is synthesized via a substitution reaction whereby MWCNT are atomically replaced by BN as described previously.[46] Multiwalled BNNT (MWBNNT) is then ultrasonicated in ethanol solution and drop-casted onto a 3 mm holey carbon on copper TEM grid. The sample is then transferred to a single-tilt specimen holder and inserted into an aberration-corrected ETEM operating at 80 keV. A total of 48 BNNTs are studied with the typical nanotube size ranging from 35 to 60 nm in diameter and from 40 to 100 walls on each nanotube.

The experiment is conducted by directing the electron beam at controlled dose rates on a MWBNNT over vacuum and measuring time for initial damage of the sample. The beam area ranges from $1.8 \times 10^4$ to $8.0 \times 10^6$ $nm^2$ with a median beam size of $3.2 \times 10^5$ $nm^2$. Pressure-limiting apertures enable $O_2$ pressures ranging from $3 \times 10^{-5}$ to $1 \times 10^2$ Pa inside the TEM specimen area. A charge coupled device (CCD) is used to record sequential images for data analysis. Refer to the Supporting Information for electron dose considerations.

**2.2. Computations.** AIMD simulations are performed using the Vienna ab initio simulation package (VASP)[47] using the projector augmented-wave (PAW) method. Static relaxations of structures are performed using plane-wave and energy cutoffs consistent with the Materials Project.[48] The energy of molecular $O_2$ adsorption is calculated for molecules at 0°, 30°, and 60° rotations at 0.15 or 0.25 nm distances from the lattice and on top of lattice atoms, along the bond between two lattice atoms, and in the center of the 6-membered ring. The lowest energy configuration is selected for AIMD simulations with adsorbed $O_2$. AIMD simulations are performed using non-spin-polarized calculations with a Γ-centered k-point. The time step is set to 1 fs. Initial single- and double-layer graphene (Gr) and h-BN lattices are statically relaxed and set to a temperature of 0 K. An initial velocity is assigned to C, B, or N lattice atoms to model the absorption of energy from incident electrons, and the minimum velocity required to eject the atom from the lattice is recorded to an accuracy of at least ±0.0025 nm/fs. The threshold energy required for nuclear displacement ($E_{n,\text{thresh}}$) is calculated as

$$E_{n,\text{thresh}} = \frac{1}{2} m_n {v_{\text{initial}}}^2 \tag{3}$$

where $m_n$ is the atomic mass of the lattice atom and $v_{\text{initial}}$ is the initial velocity assigned at the start of the AIMD simulation. For the single-layer (1-L) model, the atoms are assigned a velocity parallel to the *c*-axis, whereas for the double-layer (2-L) model, the atoms are assigned, as an initial model, a velocity at an angle so that the atom ejected from the first layer has an initial velocity vector directed at the center of the 6-fold hollow of the second layer, ⟨223⟩. The 2-L model is further refined as described in the Supporting Information to search for possible lower threshold energies. The lowest $E_{n,\text{thresh}}$ calculated from each model are reported.

## 3. RESULTS AND DISCUSSION

**3.1. Damage by Electron Dose vs $O_2$ Pressure.** Degradation experiments are performed on MWBNNTs supported on holey carbon in the TEM shown in Figure 1a. Figure 1b shows a high-resolution image of BNNT sidewalls over vacuum in the support film. A cross-sectional schematic of the sample setup in the specimen port of the ETEM is shown in Figure 1c. More details are provided in the Methods section.

The effect of varying oxygen dose under electron irradiation is analyzed. Initial experiments in an oxygen environment without the electron beam show no visible degradation with time ($t$) (see Figure S1). Figure 2 shows a tableau of degradation at increasing oxygen pressures with a constant electron dose around $5 \times 10^4$ e $nm^{-2}$ $s^{-1}$ at $t$ = 0, 5, 10, and 15 min of exposure. No damage is observed after 15 min at $5.3 \times 10^{-5}$ Pa, but at $6.7 \times 10^{-3}$ Pa, two layers degraded in the same amount of time. When the pressure is increased to $1.3 \times 10^{-2}$ Pa, the outermost layer is observed to degrade as soon as 5 min. After 15 min of electron irradiation, at least 15 layers are damaged. This shows the damage rate has a dependency on the oxygen pressure. Experimentally, the pressure is varied, and the electron dose for damage at each pressure range is recorded.

The cumulative results from the methodical observation of initial damage are organized in Figure 3. Each point represents the electron dose when initial damage to the outermost nanotube wall is first observed, an example of which is shown in Figure 2j. Blue triangles represent BNNT data from this work, and black circles represent CNT data obtained from the


https://doi.org/10.1021/acs.jpcc.4c03814
J. Phys. Chem. C 2024, 128, 18328−18337

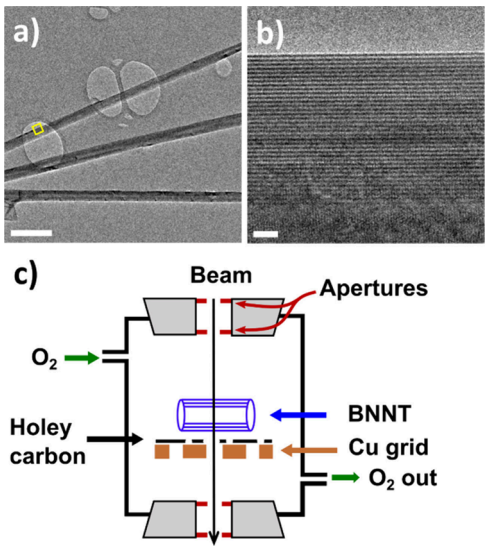


**Figure 1.** Overview of experimental setup. High-resolution TEM images of a multiwalled boron nitride nanotube (BNNT) at (a) low and (b) high magnifications. A view at 8.4K× magnification is shown in (a) and the magnified region of the BNNT sidewall at 200K× of the yellow box in (a) is shown in (b). A schematic of the microscope chamber (not to scale) is displayed in (c). Scale bars represent 200 and 2 nm for (a) and (b), respectively.

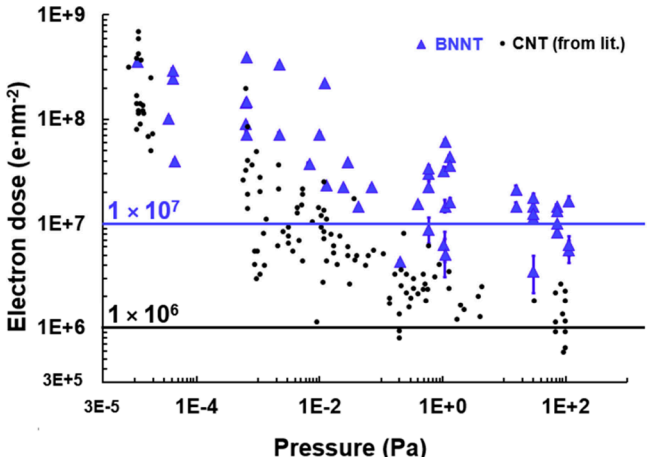


**Figure 3.** Cumulative electron dose to damage vs pressure for BNNT and CNT[24] at varying oxygen pressures. Error bars show a 10 s possible experimental deviation from the measured result. Some error bars are smaller than data symbols. CNT data adapted with permission from ref 24. Copyright 2017 Elsevier Inc.

literature.[24] At low oxygen pressures of around $5 \times 10^{-5}$ Pa, the total electron dose for damage is similar for both at an average of $1 \times 10^8$ e nm$^{-2}$. However, as the pressure increases, the amount of electron damage dose that CNT is able to withstand decreases at a faster rate than that of BNNT. At high oxygen pressures of $1 \times 10^2$ Pa, the average electron dose for damage of BNNT is approximately $1 \times 10^7$ e nm$^{-2}$ whereas CNT is approximately $1 \times 10^6$ e nm$^{-2}$, suggesting 10 times more resistance against damage for BNNT compared to CNT.

While both CNT and BNNT are van der Waals bonded between adjacent layers of tube walls, BNNT has a partially charged atomic center due to the charge difference between boron and nitrogen atoms.[49] The electrostatic interactions between layers contribute to the increased dose needed to amorphize the outermost BNNT layer, leading to the higher degradation resistance of BNNT compared to CNT. It is observed that after the initial removal of a BNNT layer, multiple adjacent layers often follow at once instead of layer-by-layer even though the first layer takes more time to remove.

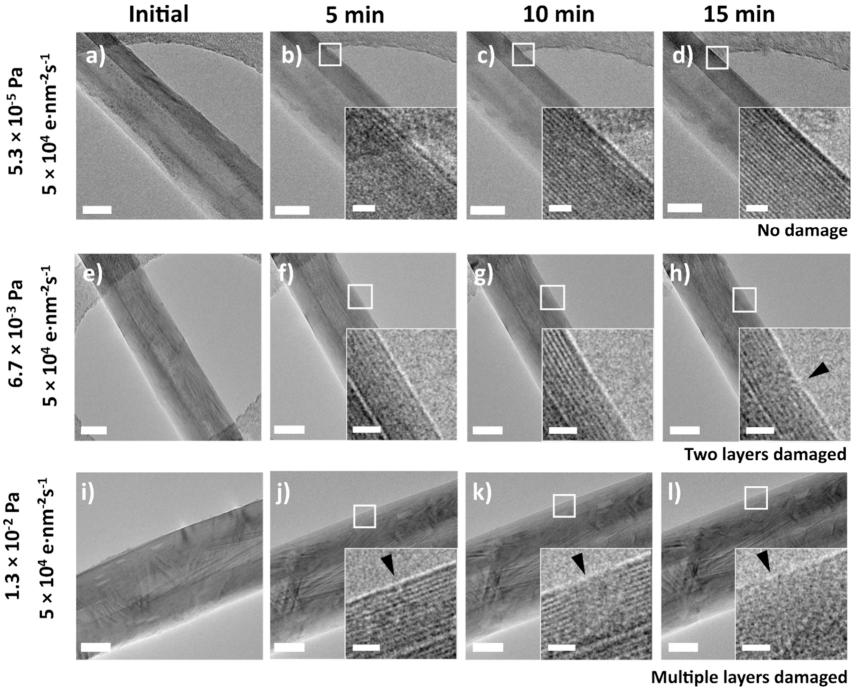


**Figure 2.** Tableau demonstrates the resistance of BNNT at different oxygen pressures with similar electron flux. (a–d) Time evolution at oxygen pressures of $4.4 \times 10^{-5}$ Pa, (e–h) at $6.7 \times 10^{-3}$ Pa, and (i–l) at $1.3 \times 10^{-2}$ Pa with an electron flux of $5 \times 10^{-4}$ e nm$^{-2}$ s$^{-1}$. Scale bars are 20 nm. Insets represent the magnified area in the square and have scale bars of 2 nm.



https://doi.org/10.1021/acs.jpcc.4c03814
J. Phys. Chem. C 2024, 128, 18328−18337

The observation may also result from the electrostatic interactions between the partially charged atomic centers between adjacent planes allowing multiple layers to be removed together.

Table 1 shows the median pressures with corresponding median electron damage dose converted to the number of electrons per boron or nitrogen atom from statistical analysis. The area of each atom is defined by the average width and height of the cross-sectional area in which each atom would be impinged by electrons on the sidewall (refer to Figure S2). The atomic area is calculated to be 0.0778 (56) $nm^2$ for BNNT and 0.0767 (55) $nm^2$ for CNT. Results confirm around 1 order of magnitude difference in electron dose resistance for BNNT compared to CNT for most of the pressure range.

**Table 1. Median Pressure at Each Magnitude and Corresponding Median Electron Dose to Damage for BNNT and CNT[a]**

| $O_2$ pressure (Pa) | damage dose CNTs ($\times 10^5$ $e^-$/at.) | damage dose BNNTs ($\times 10^5$ $e^-$/at.) |
|---|---|---|
| $3 \times 10^{-4}$ (base) | 18.41 ± 0.41 | 115.17 ± 4.41 |
| ⋮ | – | – |
| $1 \times 10^{-2}$ | 5.37 ± 0.21 | 56.40 ± 2.16 |
| $3 \times 10^{-1}$ | 2.53 ± 0.06 | 14.97 ± 0.57 |
| $1 \times 10^{0}$ | 2.10 ± 0.05 | 25.48 ± 0.98 |
| $3 \times 10^{1}$ (heating at 250 °C) | – | 78.97 ± 1.05 |
| $3 \times 10^{1}$ | 1.26 ± 0.03 | 11.55 ± 0.44 |
| $1 \times 10^{2}$ | 0.80 ± 0.02 | 4.85 ± 0.19 |

[a]All experiments are performed at room temperature unless otherwise specified. CNT data adapted with permission from ref 24. Copyright 2017 Elsevier, Inc.

Heating experiments are also conducted at a pressure range of $3 \times 10^1$ Pa. The BNNT sample is heated to 250 °C using a microelectromechanical system (MEMS) heating holder (refer to the Materials and Methods). The damage dose obtained is (78.97 ± 1.05) $\times 10^5$ $e^-$/at., shown in Table 1. This dose is more than 7 times higher than BNNTs at room temperature in the same pressure range. This contrasts the generally expected trend for thermal degradation without electron beam, where damage is typically observed at higher temperatures:[50,51] from 400 to 500 °C for CNTs[52] and from 800 to 900 °C for BNNTs.[53,54] The reason for this increased resistance to electron beam damage at elevated temperatures will be discussed in Section 3.5.

**3.2. Direct Comparison of Electron Dose vs $O_2$ Dose.** For further analysis, it is instructive to directly compare the effect of electron dose per area of a surface atom with the effect of oxygen dose per atom area for damage to occur. This is achieved by calculating the oxygen impingement rate[55,56] from oxygen pressure and the average atomic cross-sectional area of the atoms on the nanotube (refer to Figure S2). These calculated values allow us to convert oxygen pressure and exposure time into oxygen dose per atom area. The electron dose is also recalculated in terms of atom area. Refer to the Supporting Information for additional details.

Figure 4 shows the log−log plot of cumulative electron dose (Σ) where damage initiates versus oxygen dose (Ω) for BNNT and CNT.[24] Power law curves fitted to the data are not predictive but serve to illustrate the general trend observed. Both types of nanotubes show a two-slope behavior distinguished by the relative arrival rates of electrons and $O_2$ molecules, denoted by Region 1 and Region 2, as shown in Figure 4. The point of transition occurs at Σ = 10 Ω, where the electron dose is 10 times that of the oxygen dose.

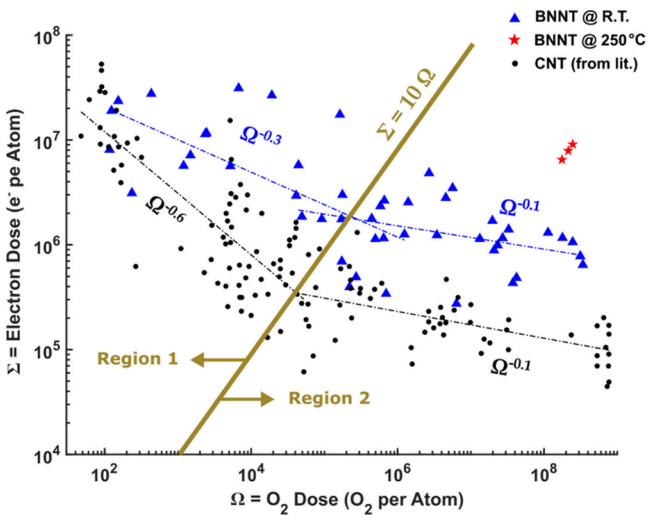


**Figure 4.** Electron dose (Σ) vs oxygen dose (Ω) comparison for CNT and BNNT. Values from BNNT heating at 250 °C are also included. Data are fitted with power law functions for Regions 1 and 2, which are oxygen-limited and electron-limited regions, respectively. CNT data adapted with permission from ref 24. Copyright 2017 Elsevier Inc.

The slopes for both nanotubes in Region 1 are steeper than those of Region 2. In Region 1, the slope for BNNT is −0.31 ± 0.03, approximately half the exponent of CNT's −0.61 ± 0.01, indicating that BNNTs are not as susceptible to degradation with increasing oxygen dose. In Region 2, the slopes transition into similar exponents for both BNNT and CNT of −0.12 ± 0.02 and −0.13 ± 0.02, respectively, which shows a significantly reduced dependence on oxygen dose. Similar slope exponents suggest that the damage becomes more electron-limited in Region 2, whereas it is oxygen-limited in Region 1. Throughout Region 1, the damage dose shows a strong dependence on oxygen pressure, implying that extrapolating down to ultrahigh-vacuum pressures would greatly decrease electron-induced damage in TEM when imaging of nanotubes with an 80 keV electron beam.

The implication for both regions is that the degradation is primarily triggered by the impact of electron interactions, with no evidence of sustained deflagration or burning of either CNT or BNNT, as would be the case for damage rate determined purely by oxygen dose.

**3.3. Analysis of Degradation Mechanics.** We now consider the kinetics of the degradation phenomenon. Our first question is whether the degradation is mainly facilitated by adsorbed $O_2$ species or by the impingement of ionized oxygen ($O_2^+$, $O^+$, etc.) in the environment. A study that analyzed images before and after plasma treatment shows that the oxygen plasma etching of graphite preferentially starts at the existing defects and generally shows poor performance in etching pristine graphite,[57] similar to other studies.[58,59] Preferential etching at defects and edges is also demonstrated for BNNT,[60,61] whereas in the work reported here we limit our observations to damage initiating at defect-free sidewalls, due to the long BNNTs and low density of defects in our specimens. Typical oxygen plasma processing pressures are in the range of 20 Pa, which follows pressures in Region 2 of


https://doi.org/10.1021/acs.jpcc.4c03814
J. Phys. Chem. C 2024, 128, 18328−18337

Table 2. Nuclear Threshold Displacement Energy ($E_{n,\mathrm{thresh}}$) in eV and Electron Threshold Energy ($E_{0,\mathrm{thresh}}$) in keV of Atoms C, B, and N for Pristine and $O_2$ Adsorbed Surfaces of Gr and h-BN Single-Layers (1-L) and Double-Layers (2-L)

| | | pristine (1-L) | | $O_2$ adsorbed (1-L) | | pristine (2-L) | | $O_2$ adsorbed (2-L) | |
|---|---|---|---|---|---|---|---|---|---|
| structure | atom | $E_{n,\mathrm{thresh}}$ | $E_{0,\mathrm{thresh}}$ | $E_{n,\mathrm{thresh}}$ | $E_{0,\mathrm{thresh}}$ | $E_{n,\mathrm{thresh}}$ | $E_{0,\mathrm{thresh}}$ | $E_{n,\mathrm{thresh}}$ | $E_{0,\mathrm{thresh}}$ |
| graphene | C | 22.3 | 121.9 | 21.2 | 115.8 | 22.6 | 123.5 | 19.1 | 104.8 |
| boron nitride | B | 20.4 | 100.6 | 19.9 | 98.3 | 26.7 | 131.3 | 25.7 | 126.4 |
| | N | 22.8 | 145.6 | 17.5 | 111.8 | 21.4 | 136.5 | 12.9 | 82.3 |

Figure 4. However, our observed damage dose shows only weak dependence on oxygen pressure in this region. In addition, electron energy loss spectroscopy (EELS) is performed on BNNT before and after oxygen-assisted beam damage to confirm that oxidation does not play a critical role, as oxygen is not observed as a statistically significant component in the EELS spectrum on the damaged BNNT after returning to vacuum conditions (refer to Figure S3). The damaged BNNT remains stoichiometric amorphous BN, without conversion to, e.g., $B_2O_3$. Therefore, we assign a low significance to the role of energetic oxygen ions on BNNT degradation.

Now, we turn our attention to adsorbed oxygen species. The energy of physisorption of $O_2$ on CNT and BNNT surfaces is 0.038 and 0.034 eV, respectively.[62,63] The base pressure in the ETEM is such that a saturated monolayer of oxygen should be readily physisorbed on exposed surfaces at room temperature, where $k_BT$ is approximately 0.026 eV. However, the recoil of electron interactions should readily desorb such weakly bound species. This creates a dynamic state yielding equilibrium adsorption of a partial monolayer, with a fractional population determined by the relative arrival rates of $O_2$ molecules and energetic electrons. At high pressures, where $O_2$ arrives at a higher rate than imaging electrons, we expect to have a fractional physisorbed monolayer approaching 100%, and indeed, we see a weak power law dependence for the damage−dose in this regime (see Figure 4), consistent with high coverage, independent of $O_2$ pressure. This suggests that the occurrence of such a monolayer plays a role in the damage pathway, although additional mechanisms are required, as the physisorption itself cannot result in damage.

We now focus on the energetic electrons and their possible damage mechanisms for the nanotubes. These mechanisms include beam heating, Coulombic charging effects, radiolysis, and knock-on damage. Beam heating effects do not heavily affect this system, as beam-induced heating experiments on carbon films show only a few °C increase at similar energy ranges and dose rates,[27] and CNT and BNNT are known to have high thermal conductivity.[64,65] Further, the results shown in Table 1 indicate that moderate heating reduces damage. Therefore, we do not expect beam heating to aggravate damage. Turning to Coulombic charging effects, we note that the nanotube is supported by a conducting carbon substrate, which together with the ambient gas environment should effectively mitigate charge buildup. Radiolysis is more complex for first principle calculations,[27,66] so we limit the discussion to knock-on mechanisms but will briefly return to radiolysis in a later discussion.

**3.4. Damage Threshold Determination with AIMD Simulations.** To explore the effects of knock-on displacement, we perform ab initio molecular dynamics (AIMD) simulations of $O_2$ adsorption on Gr and h-BN. With small nanotubes sub-10 nm in diameter, high curvature can lead to changes in band gap[67] and increased repulsive interlayer forces.[68] The BNNTs measured in this study have an average diameter of 60 nm; therefore, the atomic models use a flat multilayered h-BN structure to approximate the outer nanotube walls, as the nanotube layer curvature effects are negligible at this diameter.

The AIMD simulations are implemented to find the displacement nuclear threshold energy ($E_{n,\mathrm{thresh}}$) required to eject an atom from its lattice position. To obtain $E_{n,\mathrm{thresh}}$, we provide a target atom in the lattice with some initial velocity, and the minimum velocity required for atom ejection is determined by sampling a range of velocity values. With $E_{n,\mathrm{thresh}}$ for the atom, one can then obtain the incident electron threshold energy ($E_{0,\mathrm{thresh}}$), the minimum kinetic energy required for an electron to knock out an atom from the lattice site. Simulations of single-layer (1-L) and double-layer (2-L) h-BN and Gr lattices are implemented for this study.

Furthermore, cases with and without $O_2$ adsorption on the surface are analyzed. Because $O_2$ physisorption is shown to have no significant effect on knock-on thresholds, $E_{n,\mathrm{thresh}}$, in AIMD simulations, we hypothesize that some physisorbed $O_2$ are converted into chemisorbed molecules with energy from the electron to overcome the chemisorption barrier of 0.187 eV.[69] In other surface systems, $O_2$ has also been demonstrated to transition from physisorption to chemisorption by way of additional energetic mechanisms.[70−72] For all AIMD models considered below, the oxygen is bonded by chemisorption (i.e., oxygen is chemically bonded to the surface), even though this would not be expected from only thermal effects, and we will come back to this point later below.

In the case of a pristine 1-L lattice, the AIMD simulations yield $E_{n,\mathrm{thresh}}$ for Gr as 22.3 eV for C-displacement—and for h-BN as 20.4 and 22.8 eV for B-displacement and N-displacement, respectively—as shown in Table 2. These values are comparable to past calculations by Bui and Kotakoski[33,34] for the h-BN monolayer. Our simulations show that for a pristine lattice, the energies to displace an atom for Gr and BN are relatively similar, with the opportunity of displacing a boron atom to be slightly higher since the $E_{n,\mathrm{thresh}}$ is slightly lower. For the case of oxygen physisorption, these $E_{n,\mathrm{thresh}}$ values are not different from the pristine case. For an $O_2$ molecule chemisorbed to the surface of the 1-L lattice, the calculated $E_{n,\mathrm{thresh}}$ for Gr is 21.2 eV for C and for h-BN are 19.9 and 17.5 eV for B and N, respectively (Table 2). The $E_{n,\mathrm{thresh}}$ has not changed drastically for C and B atoms, but the change calculated for N is significant, with an $E_{n,\mathrm{thresh}}$ reduction of 5.3 eV. The trend persists for the 2-L calculations, where N shows the lowest $E_{n,\mathrm{thresh}}$ after $O_2$ chemisorption, with a reduction of 8.5 eV from the pristine lattice. This is surprising because N has a larger mass and would be expected to have a higher threshold for ejection. However, the interaction with the second layer can have a large effect, amplifying differences in atomic radius and bonding preferences (refer to Sections S5 and S6 and Videos S1 and S2).



https://doi.org/10.1021/acs.jpcc.4c03814
J. Phys. Chem. C 2024, 128, 18328−18337

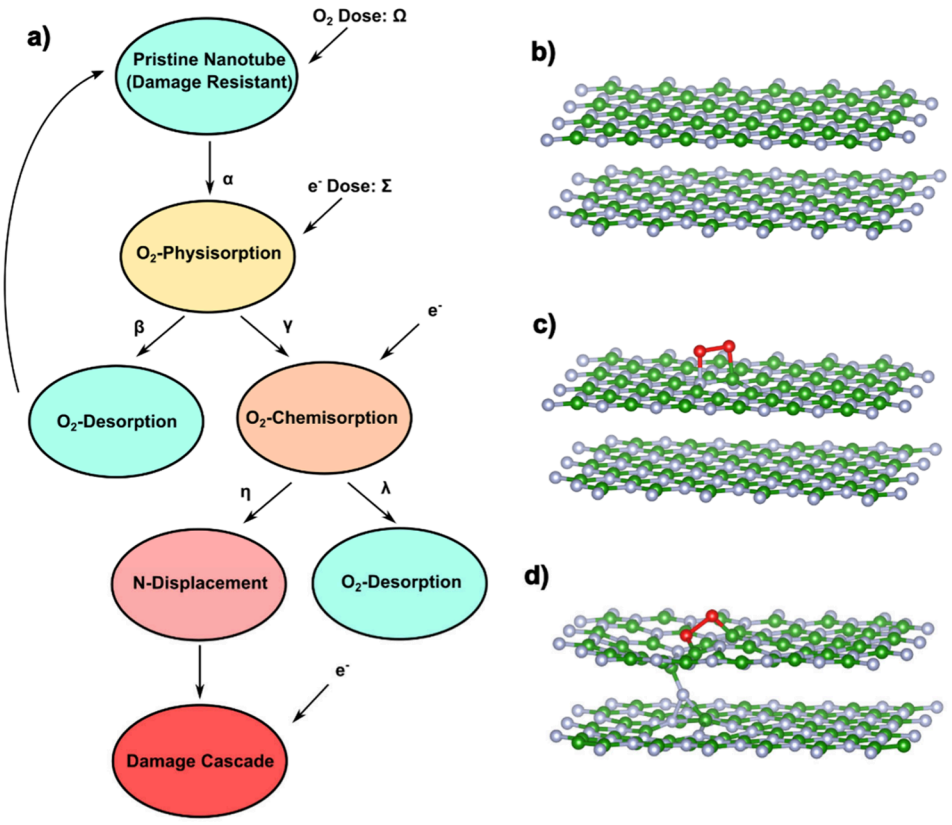


**Figure 5.** Nanotube surface interaction for atomic displacement. (a) Displacement pathway for electron-induced degradation for BNNT in an oxygenated environment. Rates $\alpha$, $\beta$, $\gamma$, $\eta$, and $\lambda$ are described in the subsequent section. (b–d) show models for AIMD simulations as follows: (b) two pristine layers of BN lattice, (c) an oxygen molecule adsorbed onto the BN surface layer, and (d) an N displacement of the surface layer above $E_{n,\text{thresh}}$ enabled by $O_2$ chemisorption.

Now, we convert these nuclear thresholds into $E_{0,\text{thresh}}$, the incident electron threshold energy for knock-on damage. We consider the kinematics of nuclear scattering in an ideal case, where the conservation of energy and momentum are upheld by classical two-particle scattering. The maximum energy transferred to the nucleus, $E_{n,\text{max}}$ can be expressed as

$$E_{n,\text{max}} = E_0 \times \frac{4m_e}{Au} \tag{1}$$

where $m_e$ is electron mass, $A$ is the atomic number, and $u$ is the atomic mass unit. This equation can be rewritten to express the threshold electron energy ($E_{0,\text{thresh}}$) as

$$E_{0,\text{thresh}} = E_{n,\text{thresh}} \times \frac{Au}{4m_e} \tag{2}$$

By comparing $E_{0,\text{thresh}}$ of each damage candidate to the electron beam energy utilized, one can determine if $O_2$-assisted knock-on is a viable degradation pathway.

The results of our analysis show 2-L $O_2$ adsorbed $E_{0,\text{thresh}}$ to be 104.8 keV for C of Gr, 126.8 keV for B of h-BN, and 82.3 keV for N of h-BN. An electron beam energy of 80 keV is used for both this study of BNNT and the study done of CNT by Koh et al.[24] From the results, we observe that $O_2$ chemisorption aids in lowering the threshold for degradation. Most notably, 2-L $O_2$-adsorbed N have an $E_{0,\text{thresh}}$ closest to 80 keV, with a value of 82.3 keV. As these calculations are performed at 0 K, the thermal effects are not considered. This indicates that N displacement in the vicinity of chemisorbed oxygen is the most likely mechanism for which our 80 keV imaging is nearest to the damage threshold. For 2-L $O_2$ adsorbed C in Gr, the $E_{0,\text{thresh}}$ is 104.8 keV; therefore, 80 keV electron beam energy is less likely to damage pristine MWCNT walls compared to MWBNNT, though thermal effects could also come into play. This correlates with previous calculations by Egerton et al. regarding Gr.[27] Damage observed for CNT could be due to higher energy configurations at the cap and cap edge, where there are heptagonal and pentagonal arrangements of carbon.[73] These are seen to also be the preferred locations where degradation is consistently observed for MWCNT.[24]

Figure 5a schematically depicts a heuristic model of the damage pathways, ultimately leading to knock-on damage. Frames of the damage sequence from AIMD simulations are demonstrated in Figure 5b–d. Initially, $O_2$ physisorbs onto the pristine BNNT surface with $O_2$ dose, as shown in Figure 5b,c. With a directed electron beam on the nanotube surface, some $O_2$ desorbs. When a higher $O_2$ pressure is reached, some molecules will remain on the surface and maintain an equilibrium concentration. Physisorbed $O_2$ can also convert into chemisorbed $O_2$ species with electron dose. This lowers the electron threshold energy necessary for a displacement of N atoms from the lattice, as shown in Figure 5d. With prolonged electron impingement, an intralayer damage cascade will initiate, leading to subsequent layer damage involving all components, as seen in other studies of both h-BN and CNT.[24,33] This cascade produces the amorphous regions that we observe in HRTEM and causes them to grow over time. In



https://doi.org/10.1021/acs.jpcc.4c03814
J. Phys. Chem. C 2024, 128, 18328−18337

the case of CNTs, degradation can preferentially initiate on the tube cap and cap edge due to the higher energy pentagonal and heptagonal C orientation at these locations, lowering the necessary electron energy threshold.[73]

**3.5. $O_2$ Desorption Study with Heating.** In order to test the proposed pathway, a heating experiment is performed at a temperature of 250 °C, which is higher than the temperature needed for desorption of a physisorbed $O_2$ molecule ($T_{des}$) given by $T_{des} > \frac{E_{O2,ads}}{k_B}$, where energy for $O_2$ adsorption, $E_{O2,ads}$ = 0.034 eV.[63] The result is shown in Table 1, where we see a 7-fold increase in the electron dose needed for degradation at the higher $O_2$ pressure. Though the pressure is measured at $3 \times 10^1$ Pa, the sample is able to withstand a higher dose than a similar BNNT sample at a pressure of $3 \times 10^{-2}$ Pa at room temperature, which is 3 magnitudes lower in pressure. Through this experiment, we demonstrate that with $O_2$ thermal desorption from the BNNT surface, the tube becomes less prone to damage, especially since the lowering of threshold energies due to atomic vibrations should increase damage at elevated temperatures.[37] This indicates that the adsorption of $O_2$ on the nanotube surface is necessary to facilitate the observed knock-on damage. It is worth noting that with Gr in vacuum conditions and at a higher temperature range than studied here, adatom or vacancy diffusion has been attributed as the mechanism for increased radiation hardness.[74,75] However, the covalent bonding of h-BN makes defect healing through vacancy diffusion a less favorable pathway.

We now consider the rates for damage reactions outlined in Figure 5a. The rate $\alpha$ for $O_2$ physisorption is the $O_2$ arrival rate, with a probability of physisorption near 100% on the lattice. With the obtained $E_{n,thresh}$ and Banhart's equation[76] for displacement cross section ($\sigma$), we can calculate the damage cross section for each atom in the lattice. At an electron beam energy of 80 keV for an h-BN lattice, $\sigma_N$ = 14.31 barn. As expected, $O_2$ adsorbed 2-L $\sigma_B$ for h-BN and $\sigma_C$ for Gr have no positive value, denoting no damage cross section for these atoms in their respective lattice at this electron energy. We can compare $\sigma_N$, which relates to the rate $\eta$ in Figure 5a, to the $O_2$ desorption rate, $\sigma_\beta$ (related to rate $\beta$ in Figure 5a), calculated to be around $1.5 \times 10^5$ barn. This indicates that $O_2$ desorption is a dominating rate in the reaction as a consequence, with $\sigma_\beta$ around 10% of the area taken by an $O_2$ molecule on a saturated, physisorbed $O_2$ monolayer. However, with prolonged electron dose flux, $O_2$ chemisorption will occur with some low probability, yielding a rate $\gamma$, which will subsequently result in either further $O_2$ desorption ($\lambda$) or N displacement ($\eta$), with further electron dose. Our model does not predict the induced chemisorption rate $\gamma$, but any nonzero value would allow the pathway to proceed. These rates give a heuristic picture of the damage mechanism, though this knock-on model might not reveal the full picture, as radiolysis could also come into play, which is highlighted by the recent work from Bui et al.[34] Currently, 2D materials do not have a comprehensive model to understand radiolysis.[37] We hope future work can address this knowledge gap, with quantitative estimates of parameters $\gamma$, $\lambda$, and $\eta$.

## 4. CONCLUSION

Our experiments show BNNT to withstand more electron radiation throughout the $O_2$ pressure range studied than CNT before damaging, often with 1 order of magnitude increase in resistance. The electron beam serves primarily as an $O_2$ desorption mechanism but has a small probability to induce knock-on effects on the BNNT sidewall. Adsorbed $O_2$ is the main facilitator of damage, and the same degradation pathway is demonstrated across the pressure range studied. The atomic displacement of N via knock-on is responsible for damage on a pristine BNNT at an electron beam of 80 keV. At higher energies (e.g., 150 keV), damage could stem from either B or N. This work gives fundamental insight into the interaction of BNNT with electron beam in an oxygenated environment and provides a direct comparison to CNT in a similar environment. Our study provides understanding of BNNT degradation mechanisms and provides credence for BNNT as a radiation-resistant material. Future work can build upon this model to determine additional contributors for radiation damage and further evaluate if the damage resistance can be maintained for other BNNT-containing composite materials.

## ■ ASSOCIATED CONTENT

### Data Availability Statement

Research data from this project will be archived at the Digital Repository at the University of Maryland (DRUM) upon manuscript publication. DRUM is a long-term, open-access repository managed and maintained by the University of Maryland Libraries. Researchers, and the general public can download data and code files, associated metadata and documentation, and any guidelines for reuse. All records in DRUM are assigned a persistent DOI to support consistent discovery and citation. The project description will be automatically indexed in Google and Google Scholar to support global discovery. When available, the data can be accessed at the following URL: http://hdl.handle.net/1903/33490.

### Supporting Information

The Supporting Information is available free of charge at https://pubs.acs.org/doi/10.1021/acs.jpcc.4c03814.

(1) Observations without beam (in oxygen environment), (2) error and uncertainty in approximations, (3) oxidation effects, (4) nanotube selection, (5) displacement threshold energy calculation considerations, and (6) video descriptions (PDF)

Videos S1 and S2 (ZIP)

## ■ AUTHOR INFORMATION


### Corresponding Author

**John Cumings** − *Department of Materials Science and Engineering, University of Maryland at College Park, College Park, Maryland 20742, United States*; Email: cumings.umd.edu

### Authors

**Hsin-Yun Chao** − *Department of Materials Science and Engineering, University of Maryland at College Park, College Park, Maryland 20742, United States; Material Science and Engineering Division, National Institute of Standards and Technology, Gaithersburg, Maryland 20899, United States*; orcid.org/0000-0002-4490-5894

**Adelaide M. Nolan** − *Department of Materials Science and Engineering, University of Maryland at College Park, College Park, Maryland 20742, United States*

**Alex T. Hall** − *Department of Materials Science and Engineering, University of Maryland at College Park, College Park, Maryland 20742, United States*

**Dmitri Golberg** − *Centre for Materials Science and School of Chemistry and Physics, Queensland University of Technology, Brisbane City, QLD 4000, Australia; Research Centre for Materials Nanoarchitectonics, National Institute for Materials Science, Tsukuba, Ibaraki 305-0003, Japan;* orcid.org/0000-0003-2298-6539

**Cheol Park** − *Advanced Materials and Processing Branch, NASA Langley Research Center, Hampton, Virginia 23681, United States*

**Wei-Chang David Yang** − *Material Science and Engineering Division, National Institute of Standards and Technology, Gaithersburg, Maryland 20899, United States;* orcid.org/0000-0002-7481-7916

**Yifei Mo** − *Department of Materials Science and Engineering, University of Maryland at College Park, College Park, Maryland 20742, United States;* orcid.org/0000-0002-8162-4629

**Renu Sharma** − *Material Science and Engineering Division, National Institute of Standards and Technology, Gaithersburg, Maryland 20899, United States*

Complete contact information is available at: https://pubs.acs.org/10.1021/acs.jpcc.4c03814

### Notes

The authors declare no competing financial interest.

## ■ ACKNOWLEDGMENTS

H.-Y.C. and J.C. acknowledge support under the Cooperative Research Agreement between the University of Maryland and the National Institute of Standards and Technology Physical Measurement Laboratory, Award 70NANB14H209, through the University of Maryland. A.T.H. and J.C. acknowledge support from the Center for Enhanced Nanofluidic Transport (CENT), an Energy Frontier Research Center funded by the U.S. Department of Energy, Office of Science, Basic Energy Sciences, under Award # DE-SC0019112. A.M.N., A.T.H., and Y.M. acknowledge the computational facilities from the University of Maryland supercomputing resources. Certain equipment, instruments, software, or materials, commercial or noncommercial, are identified in this paper in order to specify the experimental procedure adequately. Such identification is not intended to imply recommendation or endorsement of any product or service by NIST, nor is it intended to imply that the materials or equipment identified are necessarily the best available for the purpose.

## ■ REFERENCES

(1) Park, C.; Ounaies, Z.; Watson, K. A.; Pawlowski, K.; Lowther, S. E.; Connell, J. W.; Siochi, E. J.; Harrison, J. S.; Clair, T. L. St. Polymer-Single Wall Carbon Nanotube Composites for Potential Spacecraft Applications. *MRS Proceedings* **2001**, *706*, Z3.30.1.

(2) Johnston, A. H. Radiation Damage of Electronic and Optoelectronic Devices in Space. In *4th International Workshop on Radiation Effects on Semiconductor Devices for Space Application*; Tsukuba, Japan, 2000; pp 1−9.

(3) Hernández, E.; Goze, C.; Bernier, P.; Rubio, A. Elastic Properties of C and BxCyNz Composite Nanotubes. *Phys. Rev. Lett.* **1998**, *80* (20), 4502−4505.

(4) Chen, X.; Dmuchowski, C. M.; Park, C.; Fay, C. C.; Ke, C. Quantitative Characterization of Structural and Mechanical Properties of Boron Nitride Nanotubes in High Temperature Environments. *Sci. Rep* **2017**, *7* (1), 1−9.

(5) Thibeault, S. A.; Kang, J. H.; Sauti, G.; Park, C.; Fay, C. C.; King, G. C. Nanomaterials for Radiation Shielding. *MRS Bull.* **2015**, *40* (10), 836−841.

(6) Liu, Z.; Gong, Y.; Zhou, W.; Ma, L.; Yu, J.; Idrobo, J. C.; Jung, J.; MacDonald, A. H.; Vajtai, R.; Lou, J.; et al. Ultrathin High-Temperature Oxidation-Resistant Coatings of Hexagonal Boron Nitride. *Nat. Commun.* **2013**, *4* (1), 2541.

(7) Thibeault, S. A.; Fay, C. C.; Lowther, S. E.; Earle, K. D.; Sauti, G.; Kang, J. H.; Park, C.; McMullen, A. M. Radiation Shielding Materials Containing Hydrogen, Boron and Nitrogen: Systematic Computational and Experimental Study - Phase I. *NIAC Final Report* **2012**, *1*, 1−29.

(8) Kim, J.; Lee, B.-C.; Uhm, Y. R.; Miller, W. H. Enhancement of Thermal Neutron Attenuation of Nano-B4C, -BN Dispersed Neutron Shielding Polymer Nanocomposites. *J. Nucl. Mater.* **2014**, *453* (1−3), 48−53.

(9) Reidy, K.; Varnavides, G.; Thomsen, J. D.; Kumar, A.; Pham, T.; Blackburn, A. M.; Anikeeva, P.; Narang, P.; LeBeau, J. M.; Ross, F. M. Direct Imaging and Electronic Structure Modulation of Moiré Superlattices at the 2D/3D Interface. *Nat. Commun.* **2021**, *12* (1), 1−9.

(10) Zheng, Q.; Feng, T.; Hachtel, J. A.; Ishikawa, R.; Cheng, Y.; Daemen, L.; Xing, J.; Idrobo, J. C.; Yan, J.; Shibata, N.; et al. Direct Visualization of Anionic Electrons in an Electride Reveals Inhomogeneities. *Sci. Adv.* **2021**, *7* (15), No. eabe6819.

(11) Belin, T.; Epron, F. Characterization Methods of Carbon Nanotubes: A Review. *Mater. Sci. Eng. B Solid State Mater. Adv. Technol.* **2005**, *119* (2), 105−118.

(12) Liu, B.; Wu, F.; Gui, H.; Zheng, M.; Zhou, C. Chirality-Controlled Synthesis and Applications of Single-Wall Carbon Nanotubes. *ACS Nano* **2017**, *11* (1), 31−53.

(13) Tang, D. M.; Kvashnin, D. G.; Cretu, O.; Nemoto, Y.; Uesugi, F.; Takeguchi, M.; Zhou, X.; Hsia, F. C.; Liu, C.; Sorokin, P. B.; et al. Chirality Transitions and Transport Properties of Individual Few-Walled Carbon Nanotubes as Revealed by in Situ TEM Probing. *Ultramicroscopy* **2018**, *194*, 108−116.

(14) Egerton, R. F. Control of Radiation Damage in the TEM. *Ultramicroscopy* **2013**, *127*, 100−108.

(15) Sharma, R. Experimental Set up for in Situ Transmission Electron Microscopy Observations of Chemical Processes. *Micron* **2012**, *43* (11), 1147−1155.

(16) Dutta, N. S.; Shao, P.; Gong, K.; White, C. E.; Yao, N.; Arnold, C. B. Understanding Solution Processing of Inorganic Materials Using Cryo-EM. *Opt Mater. Express* **2020**, *10* (1), 119.

(17) Cumings, J.; Zettl, A.; McCartney, M. R.; Spence, J. C. H. Electron Holography of Field-Emitting Carbon Nanotubes. *Phys. Rev. Lett.* **2002**, *88* (5), 568041−568044.

(18) Ross, F. M. Opportunities and Challenges in Liquid Cell Electron Microscopy. *Science (1979)* **2015**, *350* (6267), 1−9.

(19) Sharma, R.; Moore, E.; Rez, P.; Treacy, M. M. J. Site-Specific Fabrication of Fe Particles for Carbon Nanotube Growth. *Nano Lett.* **2009**, *9* (2), 689−694.

(20) Picher, M.; Lin, P. A.; Gomez-Ballesteros, J. L.; Balbuena, P. B.; Sharma, R. Nucleation of Graphene and Its Conversion to Single-Walled Carbon Nanotubes. *Nano Lett.* **2014**, *14* (11), 6104−6108.

(21) Lin, P. A.; Gomez-Ballesteros, J. L.; Burgos, J. C.; Balbuena, P. B.; Natarajan, B.; Sharma, R. Direct Evidence of Atomic-Scale Structural Fluctuations in Catalyst Nanoparticles. *J. Catal.* **2017**, *349*, 149−155.

(22) He, M.; Jiang, H.; Liu, B.; Fedotov, P. V.; Chernov, A. I.; Obraztsova, E. D.; Cavalca, F.; Wagner, J. B.; Hansen, T. W.; Anoshkin, I. V.; et al. Chiral-Selective Growth of Single-Walled Carbon Nanotubes on Lattice-Mismatched Epitaxial Cobalt Nanoparticles. *Sci. Rep* **2013**, *3*, 1−7.

(23) Chao, H. Y.; Jiang, H.; Ospina-Acevedo, F.; Balbuena, P. B.; Kauppinen, E. I.; Cumings, J.; Sharma, R. A Structure and Activity Relationship for Single-Walled Carbon Nanotube Growth Confirmed by: In Situ Observations and Modeling. *Nanoscale* **2020**, *12* (42), 21923−21931.

(24) Koh, A. L.; Sinclair, R. Assessing and Ameliorating the Influence of the Electron Beam on Carbon Nanotube Oxidation in Environmental Transmission Electron Microscopy. *Ultramicroscopy* **2017**, *176*, 132−138.
(25) Banhart, F. Structural Transformations in Carbon Nanoparticles Induced by Electron Irradiation. *Phys. Solid State* **2002**, *44* (3), 399−404.
(26) Ritter, U.; Scharff, P.; Siegmund, C.; Dmytrenko, O. P.; Kulish, N. P.; Prylutskyy, Yu. I.; Belyi, N. M.; Gubanov, V. A.; Komarova, L. I.; Lizunova, S. V.; et al. Radiation Damage to Multi-Walled Carbon Nanotubes and Their Raman Vibrational Modes. *Carbon N Y* **2006**, *44* (13), 2694−2700.
(27) Egerton, R. F.; Li, P.; Malac, M. Radiation Damage in the TEM and SEM. *Micron* **2004**, *35* (6), 399−409.
(28) Egerton, R. F.; McLeod, R.; Wang, F.; Malac, M. Basic Questions Related to Electron-Induced Sputtering in the TEM. *Ultramicroscopy* **2010**, *110* (8), 991−997.
(29) Egerton, R. F. Mechanisms of Radiation Damage in Beam-Sensitive Specimens, for TEM Accelerating Voltages between 10 and 300 KV. *Microsc Res. Tech* **2012**, *75* (11), 1550−1556.
(30) Hobbs, L. W. Radiation Effects in Analysis of Inorganic Specimens by TEM. In *Introduction to Analytical Electron Microscopy*; Hren, J. J., Goldstein, J. I., Joy, D. C., Eds.; Springer US: Boston, MA, 1979; pp 437−480.
(31) Watanabe, K.; Taniguchi, T.; Kanda, H. Direct-Bandgap Properties and Evidence for Ultraviolet Lasing of Hexagonal Boron Nitride Single Crystal. *Nat. Mater.* **2004**, *3* (6), 404−409.
(32) Cretu, O.; Lin, Y. C.; Suenaga, K. Inelastic Electron Irradiation Damage in Hexagonal Boron Nitride. *Micron* **2015**, *72*, 21−27.
(33) Kotakoski, J.; Jin, C. H.; Lehtinen, O.; Suenaga, K.; Krasheninnikov, A. V. Electron Knock-on Damage in Hexagonal Boron Nitride Monolayers. *Phys. Rev. B Condens Matter Mater. Phys.* **2010**, *82* (11), 1−4.
(34) Bui, T. A.; Leuthner, G. T.; Madsen, J.; Monazam, M. R. A.; Chirita, A. I.; Postl, A.; Mangler, C.; Kotakoski, J.; Susi, T. Creation of Single Vacancies in HBN with Electron Irradiation. *Small* **2023**, *19* (39), 2301926.
(35) Alem, N.; Erni, R.; Kisielowski, C.; Rossell, M. D.; Gannett, W.; Zettl, A. Atomically Thin Hexagonal Boron Nitride Probed by Ultrahigh-Resolution Transmission Electron Microscopy. *Phys. Rev. B Condens Matter Mater. Phys.* **2009**, *80* (15), 1−7.
(36) Meyer, J. C.; Chuvilin, A.; Algara-Siller, G.; Biskupek, J.; Kaiser, U. Selective Sputtering and Atomic Resolution Imaging of Atomically Thin Boron Nitride Membranes. *Nano Lett.* **2009**, *9* (7), 2683−2689.
(37) Susi, T.; Meyer, J. C.; Kotakoski, J. Quantifying Transmission Electron Microscopy Irradiation Effects Using Two-Dimensional Materials. *Nature Reviews Physics* **2019**, *1* (6), 397−405.
(38) Kim, J. S.; Borisenko, K. B.; Nicolosi, V.; Kirkland, A. I. Controlled Radiation Damage and Edge Structures in Boron Nitride Membranes. *ACS Nano* **2011**, *5* (5), 3977−3986.
(39) Ngoc My Duong, H.; Nguyen, M. A. P.; Kianinia, M.; Ohshima, T.; Abe, H.; Watanabe, K.; Taniguchi, T.; Edgar, J. H.; Aharonovich, I.; Toth, M. Effects of High-Energy Electron Irradiation on Quantum Emitters in Hexagonal Boron Nitride. *ACS Appl. Mater. Interfaces* **2018**, *10* (29), 24886−24891.
(40) Cheng, G.; Yao, S.; Sang, X.; Hao, B.; Zhang, D.; Yap, Y. K.; Zhu, Y. Evolution of Irradiation-Induced Vacancy Defects in Boron Nitride Nanotubes. *Small* **2016**, *12* (6), 818−824.
(41) Leuthner, G. T.; Susi, T.; Mangler, C.; Meyer, J. C.; Kotakoski, J. Chemistry at Graphene Edges in the Electron Microscope. *2d Mater.* **2021**, *8* (3), 035023.
(42) Thomsen, J. D.; Kling, J.; MacKenzie, D. M. A.; Bøggild, P.; Booth, T. J. Oxidation of Suspended Graphene: Etch Dynamics and Stability beyond 1000°c. *ACS Nano* **2019**, *13* (2), 2281−2288.
(43) Åhlgren, E. H.; Markevich, A.; Scharinger, S.; Fickl, B.; Zagler, G.; Herterich, F.; McEvoy, N.; Mangler, C.; Kotakoski, J. Atomic-Scale Oxygen-Mediated Etching of 2D MoS2 and MoTe2. *Adv. Mater. Interfaces* **2022**, *9* (32), 2200987.
(44) Koh, A. L.; Gidcumb, E.; Zhou, O.; Sinclair, R. Observations of Carbon Nanotube Oxidation in an Aberration-Corrected Environmental Transmission Electron Microscope. *ACS Nano* **2013**, *7* (3), 2566−2572.
(45) Koh, A. L.; Gidcumb, E.; Zhou, O.; Sinclair, R. Oxidation of Carbon Nanotubes in an Ionizing Environment. *Nano Lett.* **2016**, *16* (2), 856−863.
(46) Kalay, S.; Yilmaz, Z.; Sen, O.; Emanet, M.; Kazanc, E. Synthesis of Boron Nitride Nanotubes and Their Applications. *Beilstein J. Nanotechnol.* **2015**, *6*, 84−102.
(47) Kresse, G.; Furthmüller, J. Efficient Iterative Schemes for Ab Initio Total-Energy Calculations Using a Plane-Wave Basis Set. *Phys. Rev. B Condens Matter Mater. Phys.* **1996**, *54* (16), 11169−11186.
(48) Jain, A.; Ong, S. P.; Hautier, G.; Chen, W.; Richards, W. D.; Dacek, S.; Cholia, S.; Gunter, D.; Skinner, D.; Ceder, G.; Persson, K. A. The Materials Project: A Materials Genome Approach to Accelerating Materials Innovation. *APL Mater.* **2013**, *1* (1), 11002.
(49) Hod, O. Graphite and Hexagonal Boron-Nitride Have the Same Interlayer Distance. Why? *J. Chem. Theory Comput* **2012**, *8* (4), 1360−1369.
(50) Seo, M. K.; Park, S. J. A Kinetic Study on the Thermal Degradation of Multi-Walled Carbon Nanotubes-Reinforced Poly-(Propylene) Composites. *Macromol. Mater. Eng.* **2004**, *289* (4), 368−374.
(51) Li, J.; Tong, L.; Fang, Z.; Gu, A.; Xu, Z. Thermal Degradation Behavior of Multi-Walled Carbon Nanotubes/Polyamide 6 Composites. *Polym. Degrad. Stab.* **2006**, *91* (9), 2046−2052.
(52) Ajayan, P. M.; Ebbesen, T. W.; Ichihashi, T.; Iijima, S.; Tanigaki, K.; Hiura, H. Opening Carbon Nanotubes with Oxygen and Implications for Filling. *Nature* **1993**, *362* (6420), 522−525.
(53) Chen, Y.; Zou, J.; Campbell, S. J.; Caer, G. Le. Boron Nitride Nanotubes : Pronounced Resistance to Oxidation. *Appl. Phys. Lett.* **2004**, *84* (13), 2430−2432.
(54) Kim, J. H.; Pham, T. V.; Hwang, J. H.; Kim, C. S.; Kim, M. J. Boron Nitride Nanotubes: Synthesis and Applications. *Nano Converg* **2018**, *5* (1), 1−13.
(55) Chapman, S.; Cowling, T. G. *The Mathematical Theory of Non-Uniform Gases*, 3rd ed.; Cambridge University Press: 1991.
(56) Kauzmann, W. *Kinetic Theory of Gases*, 1st ed.; Dover Publications, Inc.: Mineona, NY, 1966.
(57) Paredes, J. I.; Martínez-Alonso, A.; Tascón, J. M. D. Comparative Study of the Air and Oxygen Plasma Oxidation of Highly Oriented Pyrolytic Graphite: A Scanning Tunneling and Atomic Force Microscopy Investigation. *Carbon N Y* **2000**, *38* (8), 1183−1197.
(58) Chang, H.; Bard, A. J. Scanning Tunneling Microscopy Studies of Carbon-Oxygen Reactions on Highly Oriented Pyrolytic Graphite. *J. Am. Chem. Soc.* **1991**, *113* (15), 5588−5596.
(59) Chu, X.; Schmidt, L. D. Reactions of NO, 02, H20, And. *Surf. Sci.* **1992**, *268*, 325−332.
(60) Jacobson, N.; Farmer, S.; Moore, A.; Sayir, H. High-Temperature Oxidation of Boron Nitride: I, Monolithic Boron Nitride. *J. Am. Ceram. Soc.* **1999**, *82* (2), 393−398.
(61) Marincel, D. M.; Adnan, M.; Ma, J.; Bengio, E. A.; Trafford, M. A.; Kleinerman, O.; Kosynkin, D. V.; Chu, S. H.; Park, C.; Hocker, S. J. A.; et al. Scalable Purification of Boron Nitride Nanotubes via Wet Thermal Etching. *Chem. Mater.* **2019**, *31* (5), 1520−1527.
(62) Sorescu, D. C.; Jordan, K. D.; Avouris, P. Theoretical Study of Oxygen Adsorption on Graphite and the (8,0) Single-Walled Carbon Nanotube. *J. Phys. Chem. B* **2001**, *105* (45), 11227−11232.
(63) Baei, M. T.; Kaveh, F.; Torabi, P.; Sayyad-Alangi, S. Z. Adsorption Properties of Oxygen on H-Capped (5, 5) Boron Nitride Nanotube (BNNT)-a Density Functional Theory. *E-Journal of Chemistry* **2011**, *8* (2), 609−614.
(64) Kim, P.; Shi, L.; Majumdar, A.; McEuen, P. L. Thermal Transport Measurements of Individual Multiwalled Nanotubes. *Phys. Rev. Lett.* **2001**, *87* (21), 215502-1.
(65) Terao, T.; Zhi, C.; Bando, Y.; Mitome, M.; Tang, C.; Golberg, D. Alignment of Boron Nitride Nanotubes in Polymeric Composite

Films for Thermal Conductivity Improvement. *J. Phys. Chem. C* **2010**, *114* (10), 4340−4344.
(66) Arenal, R.; Stéphan, O.; Kociak, M.; Taverna, D.; Loiseau, A.; Colliex, C. Electron Energy Loss Spectroscopy Measurement of the Optical Gaps on Individual Boron Nitride Single-Walled and Multiwalled Nanotubes. *Phys. Rev. Lett.* **2005**, *95* (12), 1−4.
(67) Zólyomi, V.; Kürti, J. First-Principles Calculations for the Electronic Band Structures of Small Diameter Single-Wall Carbon Nanotubes. *Phys. Rev. B Condens Matter Mater. Phys.* **2004**, *70* (8), 1−8.
(68) Kiang, C. H.; Endo, M.; Ajayan, P. M.; Dresselhaus, G.; Dresselhaus, M. S. Size Effects in Carbon Nanotubes. *Phys. Rev. Lett.* **1998**, *81* (9), 1869−1872.
(69) Sendt, K.; Haynes, B. S. Density Functional Study of the Chemisorption of O2 on the Armchair Surface of Graphite. *Proceedings of the Combustion Institute* **2005**, *30 II* (2), 2141−2149.
(70) Puglia, C.; Nilsson, A.; Hernnäs, B.; Karis, O.; Bennich, P.; Mårtensson, N. Physisorbed, Chemisorbed and Dissociated O2 on Pt(111) Studied by Different Core Level Spectroscopy Methods. *Surf. Sci.* **1995**, *342* (1−3), 119−133.
(71) Bartolucci, F.; Franchy, R.; Barnard, J. C.; Palmer, R. E. Two Chemisorbed Species of O2 on Ag(110). *Phys. Rev. Lett.* **1998**, *80* (23), 5224−5227.
(72) Zhai, H. J.; Wang, L. S. Chemisorption Sites of CO on Small Gold Clusters and Transitions from Chemisorption to Physisorption. *J. Chem. Phys.* **2005**, *122* (5), 1−4.
(73) Khalilov, U.; Bogaerts, A.; Neyts, E. C. Atomic Scale Simulation of Carbon Nanotube Nucleation from Hydrocarbon Precursors. *Nat. Commun.* **2015**, *6* (10306), 1−7.
(74) Postl, A.; Hilgert, P. P. P.; Markevich, A.; Madsen, J.; Mustonen, K.; Kotakoski, J.; Susi, T. Indirect Measurement of the Carbon Adatom Migration Barrier on Graphene. *Carbon N Y* **2022**, *196*, 596−601.
(75) Dyck, O.; Yeom, S.; Dillender, S.; Lupini, A. R.; Yoon, M.; Jesse, S. The Role of Temperature on Defect Diffusion and Nanoscale Patterning in Graphene. *Carbon N Y* **2023**, *201*, 212−221.
(76) Banhart, F. Irradiation Effects in Carbon Nanostructures. *Rep. Prog. Phys.* **1999**, *62*, 1181−1221.


https://doi.org/10.1021/acs.jpcc.4c03814
*J. Phys. Chem. C* 2024, 128, 18328−18337